Overcoming the Limitations of Transient Photovoltage Measurements for Studying Recombination in Organic Solar Cells

Mohammed Azzouzi,* Philip Calado, Andrew M. Telford, Flurin Eisner, Xueyan Hou, Thomas Kirchartz, Piers R. F. Barnes, and Jenny Nelson*

Transient photovoltage (TPV) measurements are frequently used to study recombination processes in thin-film solar cells by probing the decay of a small optically induced voltage perturbation to infer the charge carrier dynamics of devices at open circuit. However, the validity of this method to probe organic semiconductors has recently come into doubt due to large discrepancies in the reported carrier lifetime values for the same systems and the reporting of unrealistic reaction order values. Herein, the validity of TPV to extract reliable charge carrier lifetimes in thin-film solar cells is explored through the use of time-dependent drift-diffusion simulations and measurements. It is found that in low-mobility materials, TPV serves primarily as a probe of charge carrier redistribution in the bulk rather than bulk recombination dynamics and that the extracted time constant is highly mobility dependent. To address this shortcoming, transient photocharge, a new technique to measure the charge carrier density during photovoltage decay, is introduced and applied to study the recombination dynamics in a series of (fullerene and nonfullerene) organic solar cell systems. It is shown that using this technique the charge carrier recombination lifetime in the active layer is more accurately determined.

1. Introduction

In a solar cell, charge carrier recombination acts to restore the photogenerated electron-hole pair population to its quasi-thermal equilibrium value.[1] To achieve better efficiencies, these recombination events should be minimized toward the radiative limit, i.e., where only radiative recombination events due to the reciprocity principle occur.[2,3] Characterizing and identifying the recombination mechanisms in thin-film solar cells have been important challenges for the community. To this end, several techniques have been proposed to quantify the charge carrier lifetime under different operating conditions. These include both optical and electrical transient measurements to probe the recombination kinetics of the photogenerated carriers. Transient photoluminescence (TRPL)[4] and transient absorption spectroscopy (TAS)[5] probe the charge carrier population by monitoring the kinetics of photoluminescence decay and change in charge carrier absorption, respectively. Optical measurements can probe the carrier dynamics down to pico- or even femtosecond timescales but are often difficult to carry out on a full device and under operational conditions. By contrast, while the temporal resolution of electrical measurements is limited by the device's resistance-capacitance response, transient electrical measurements can be carried out on full solar cell devices under a variety of operational conditions. Electrical measurements of carrier lifetime can be separated into two groups; 1) techniques that rely on the extracted current density after a time delay, such as time-delayed collection field (TDCF),[6–8] time-resolved charge extraction (TRCE),[9–11] and photocharge extraction by linearly increasing voltage[12,13] and 2) techniques that rely on the change in the electrochemical potential difference at the contacts, such as open-circuit voltage decay,[14–16]

M. Azzouzi, Dr. P. Calado, Dr. A. M. Telford, Dr. F. Eisner, Dr. X. Hou, Dr. P. R. F. Barnes, Prof. J. Nelson
Department of Physics and Centre for Plastic Electronics
Imperial College London
London SW7 2AZ, UK
E-mail: mohammed.azzouzi15@ic.ac.uk; jenny.nelson@imperial.ac.uk

Dr. X. Hou
School of Physics and Astronomy
Queen Mary University of London
London E1 4NS, UK

Prof. T. Kirchartz
IEK5-Photovoltaics
Forschungszentrum Jülich
52425 Jülich, Germany

Prof. T. Kirchartz
Faculty of Engineering and CENIDE
University of Duisburg-Essen
Carl-Benz-Str. 199, 47057 Duisburg, Germany

intensity-modulated voltage spectroscopy,[17,18] and transient photovoltage (TPV).

TPV relies on the measurement of the photovoltage response to a small light perturbation superimposed on a constant bias light. While for large perturbations the excess charge carrier density will depend exponentially on voltage, for small perturbations, this dependence becomes linear. In certain conditions, i.e., when the charge carrier distribution is uniform, the time derivative of the small signal change in open circuit voltage (V_{oc}) will be proportional to that of the charge carrier density. Thus, the characteristic time constant of the voltage decay is called the small-signal TPV "lifetime". It is important to note that the word lifetime in the context of recombination processes usually refers to the time constant of an exponential decay of the electron or hole concentration and that the V_{oc} decay is only used as a proxy for the electron and hole concentrations, which are not directly accessible. In this work we will refer to the TPV "lifetime" as the TPV time constant.

Since the method was first introduced by O'Regan et al.,[19] TPV has been widely used to characterize thin-film solar cells such as dye-sensitized solar cells, lead sulfide quantum dot (PbS) solar cells and organic photovoltaics (OPV), as well as metal halide perovskites.[20–27] Values of the recombination time constant obtained from TPV have been shown to agree reasonably well with TAS, impedance spectroscopy and other electric techniques in OPV devices. However, this only holds for the few studies where such comparisons were made.[5,10] TPV is often coupled with charge extraction (CE) or transient photocurrent (TPC) measurements to quantify the charge carrier density at a given applied bias. TPV and CE are typically measured at different bias light intensities to characterize the dependence of the charge carrier lifetime (τ) and the charge carrier density (n) on the open-circuit voltage of the cell under bias light before the pulse (V_{OC}). These dependences are used to extract a reaction order (δ, where the recombination rate is $R \propto n^\delta$) that helps identifying the dominant recombination mechanism.[28]

Apart from the large discrepancy of the reported values for the recombination times in the literature for similar samples, unphysical reaction orders ($\delta \gg 2$) reported in several cases have raised concerns regarding the reliability of the measurement.[29,30] Kirchartz and Nelson[28] used drift-diffusion simulations to demonstrate how spatial inhomogeneity of charge carriers can lead to the high apparent reaction orders often observed in measurements. Recently, Kiermasch et al. and Sandberg et al. provided experimental evidence that the TPV time constant is limited by capacitive effects due to the spatial separation of the photoexcited carriers in the devices.[31,32] In another recent work, Neukom et al. demonstrated, again using drift-diffusion simulations, that the recombination lifetime extracted from TPV can differ from the input bulk recombination lifetime value[33] in cases where recombination was transport limited. It appears therefore that TPV is only a reliable measure of charge carrier lifetime in particular cases: A robust method for determining the situations in which TPV is a valid measure of bulk lifetime is therefore required.

In this work, we use time-dependent drift-diffusion simulations to explore the validity of using TPV to extract reliable charge carrier lifetimes in thin-film solar cells for different device parameters. The numerical simulations allow us to distinguish

between the charge carrier density and quasi-Fermi level splitting inside the absorber layer (i.e., a chemical potential) and the voltage measured at the external contacts (an electrostatic potential difference). While the discrepancy between these two types of potentials has been noted and exploited in the past,[34] e.g., to determine the mobility or diffusion length of the charge carrier from comparison of the two quantities,[35–37] the difference has not, so far, been explicitly discussed in the context of TPV measurements. The internal quasi-Fermi level splitting and the external voltage approach each other if either no current flows (a steady-state open-circuit situation) or if the mobilities are high and therefore little gradient in the electrochemical potential is needed to drive the current in or out of the absorber layer.[38] We, therefore, first explore the effect of the charge carrier mobility in the active layer on the correlation between the input recombination rate constant and the extracted rate constant from the simulated TPV response. We show that in many low-mobility cases TPV is primarily a probe of the charge carrier redistribution in the active layer rather than the bulk recombination kinetics. We then explore the effect of additional parameters (such as the energy-level mismatch between the layers and the generation rate constant) and rationalize the results using an analytical approximation for the TPV time constant when controlled by charge carrier dynamics close to the interfaces. Finally, we use our improved understanding of the processes affecting the voltage transients to introduce a modified TPV technique: transient photocharge (TPQ). This technique allows us to reliably measure the recombination lifetime of the charge carriers in the bulk by probing the charge density in the device during TPV. TPQ was applied first to poly(3-hexylthiophene) (P3HT):phenyl-C_{61}-butyric acid methyl ester (PCBM) and P3HT:O-IDTBR(full name in the Supporting Information, section S13) solar cells, as examples of thin-film solar cells, where TPV may be mobility limited. Then we measured the lifetime using both TPV and TPQ for three high-efficiency nonfullerene-based organic solar cells.

2. The Limitations of TPV

2.1. Simulation Model

To investigate and understand the factors limiting the validity of using TPV to assess the recombination lifetime in a solar cell, we begin by simulating typical TPV measurements and comparing our input parameters with the parameters extracted by applying the commonly used TPV analysis to the simulated device response. We will initially focus our study on one type of device structure, p-type(hole transport layer [HTL])/intrinsic(absorber)/ n-type(electron transport layer [ETL]) (p-i-n), which is often found in various thin-film solar cell technologies, where TPV is used as a characterization tool (such as in OPV and perovskite photovoltaics).[39–43]

Three main recombination mechanisms can limit the performance of solar cells[1,41]: direct recombination between a free electron and a free hole,[44] recombination mediated through a trap state,[45] and Auger recombination[46] (which is generally not relevant to organic solar cells under normal operational conditions). The rate of these recombination mechanisms can be simulated by considering a rate constant, the charge carrier densities, and the

reaction order of the process. In this work we will focus on the first two mechanisms: a special case of trap-assisted recombination described by the Shockley–Read–Hall (SRH) formalism with a trap state energy in the middle of the gap[28] and direct second-order recombination.[1] We will refer to the recombination rate constants used as inputs to the simulations as k_{SRH}^{input} in s^{-1} for the SRH process and B^{input} in cm^3 s^{-1} for the second-order process. A detailed derivation of the equations relating the recombination rate to the TPV time constant for the two recombination mechanisms considered is presented in the Supporting Information, section 1. For the case of trap-assisted recombination, the input recombination rate constant is related to the TPV time constant through $k_{SRH}(\tau_{TPV}) = 1/2\tau_{TPV}$ (where τ_{TPV} is the TPV time constant). For the second-order recombination mechanism the recombination lifetime is dependent on the charge carrier density. The TPV time constant is therefore related to the input recombination rate constant using $B(\tau_{TPV}) = 1/2\tau_{TPV}n_{avg}$, where n_{avg} is the average excess charge carrier density in the device under light. Experimentally, n_{avg} can be measured by CE (i.e., integrating the large perturbation photocurrent response with time at short circuit or under reverse bias)[23] or carrying out a differential capacitance CE measurement.[47] Using each recombination type, we cover two cases, one in which the charge carrier lifetime is independent of the charge carrier concentration in the device (first order recombination) and one in which the observed charge carrier recombination lifetime is expected to depend on the charge carrier concentration (second-order recombination). The results of the simulation presented below can similarly be expanded to any recombination mechanism independent of its recombination order.

The model presented here does not include the effect of trap states on the accumulation of charges in the bulk, which has often been used to explain the high apparent recombination reaction orders extracted from transient optoelectronic measurements.[28,48] We neglected this effect to demonstrate that even in the simplest case the TPV time constant is not solely related to the recombination parameters of the device. A discussion of the effect of bulk trap states on the simulated TPV experiment is presented in the Supporting Information, section 12. However, we expect the analysis that we present later to be valid for measurements of a system containing trapped charges in the bulk, under dynamic equilibrium conditions. Because the measurements are carried out and analyzed in the small perturbation regime, the input recombination rate constant and mobility would then refer to the effective charge density-dependent values.[35]

2.2. Simulation Results

2.2.1. How Does Charge Carrier Mobility Influence TPV Measurements?

First, we simulate the TPV experiment for devices with similar recombination properties and different values of charge carrier mobility in the absorber layer (μ) (assumed to be the same for holes and electrons). **Figure 1** shows the TPV time constant extracted from the simulated devices with three different values of μ as a function of the uniform generation rates. Figure 1a shows the results for three devices where the dominant recombination mechanism is SRH with $k_{SRH}^{input} = 1.8 \times 10^6$ s^{-1}. Our first observation is that while the recombination properties are similar for the three devices, their TPV time constants are significantly different for most of the generation rates considered. For the devices where the SRH recombination mechanism dominates, the TPV time constant is not necessarily constant with the generation rate, in contrast to what would be expected for a first-order recombination mechanism. We observe that the TPV time constant for these three devices (with different charge carrier mobilities) converges to the value that is expected from the input rate constant only at high light intensities, whereas for the devices where second-order recombination dominates (Figure 1b), the TPV time constant is different for different mobilities for all light intensities considered, even though the input recombination coefficient is the same. The TPV time constants show a surprising dependence on the mobility of charge carriers for both first-order (Figure 1a) and second-order (Figure 1b) recombination.
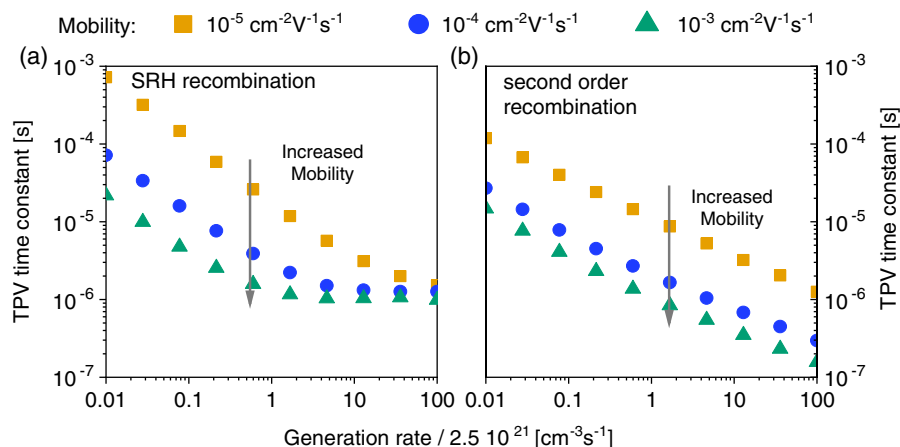

Figure 1. Extracted TPV time constant from the simulated TPV experiment of three devices with a similar recombination rate constant but different charge mobilities as a function of uniform charge carrier generation rate. a) A device with SRH recombination, $k_{SRH}^{input} = 1.8 \times 10^6$ s^{-1}. b) A device with second-order recombination, $B^{input} = 8.8 \times 10^{-11}$ cm^3 s^{-1}. A generation rate of 2.5×10^{21} cm^{-3} s^{-1} is approximately equivalent to 1 sun illumination. Additional device simulation parameters are given in the Supporting Information.
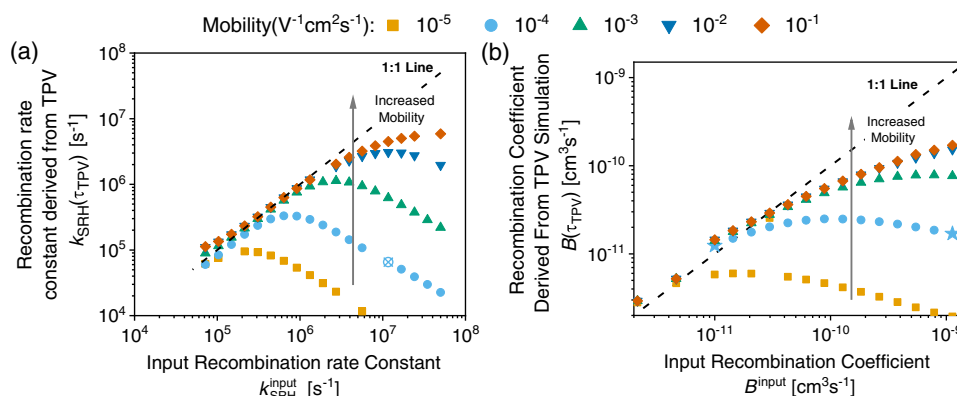
Figure 2. Simulated TPV decay rate constant against input recombination rate coefficient for different mobility values and a uniform generation rate ($G = 2.5 \times 10^{21}$ cm^{-3} s^{-1}) in a device dominated by a) first-order and b) second-order bulk recombination mechanisms. k_{SRH}^{input} and B^{input} are the input recombination rate constants for first-order and second-order recombination processes, respectively. $k_{SRH}(\tau_{TPV})$ and $B(\tau_{TPV})$ are the recombination rate constants estimated from the simulated TPV decays using the TPV time constant for first-order and second-order recombination, respectively. The star symbols show the cases considered in the Section 2.2.2 as the fast and slow recombination cases. The crossed symbol in discussed in the main text.

These initial results show that charge carrier mobility significantly affects the TPV time constant even though it does not affect the recombination rate constants in the simulated devices. The effect of charge carrier mobility on the TPV time constant has been observed in simulations reported by both Neukom et al. and Wood et al.[33,49] However, neither study explored the extent to which the charge carrier mobility affects the TPV time constant. In this work, we first focus on the dependence of the TPV time constant on charge carrier mobility to investigate the limitations of the TPV technique to extract a reliable recombination rate constant. To do so, we first compare the input recombination rate constant to the extracted recombination rate constant from the results of simulated TPV experiments for a range of charge carrier mobilities. **Figure 2** shows the result of TPV simulation using the parameter set given in Table S1, Supporting Information, with varying recombination parameter inputs and different charge carrier mobilities in the absorber layer, for the SRH recombination mechanism (Figure 2a) and second-order recombination mechanism (Figure 2b).

The figure compares the input recombination rate constant (B^{input} or k_{SRH}^{input}) to that estimated from the simulated TPV decay ($B(\tau_{TPV})$ or $k_{SRH}(\tau_{TPV})$). In Figure 2, the dashed line represents the case where the measured TPV recombination rates equal the (simulated) intrinsic recombination rate. All the simulated TPV decays were in a monoexponential form, such that a single value of τ_{TPV} fully characterizes the decay, i.e., two TPV decays with similar time constants are indistinguishable (Figure S1, Supporting Information). The results in Figure 2 show that both recombination mechanisms show a similar behavior. For the case where the mobility is of the order 10^{-1} cm^2 V^{-1} s^{-1} (orange diamonds), which would be among the highest for organic semiconductors,[50] the input and extracted values from the TPV experiment are quite similar over the range of values of B^{input} or k_{SRH}^{input} investigated. In this case, the estimated $B(\tau_{TPV})$ or $k_{SRH}(\tau_{TPV})$ values only deviate from the input parameter values for the highest recombination rate constants. However, in the simulated devices with lower charge carrier mobilities in

the absorber (μ), $B(\tau_{TPV})$ and $k_{SRH}(\tau_{TPV})$ deviate significantly from the input recombination rates. For example, for the cases with $\mu = 10^{-4}$ cm^2 V^{-1} s^{-1} (light blue circles), $B(\tau_{TPV})$ and $k_{SRH}(\tau_{TPV})$ are similar to B^{input} and k_{SRH}^{input} for low values of the recombination rate input, whereas for $k_{SRH}^{input} > 10^6$ s^{-1} and $B^{input} > 3 \times 10^{-11}$ cm^3 s^{-1}, $B(\tau_{TPV})$ and $k_{SRH}(\tau_{TPV})$ deviate significantly from the expected value. For instance, in the device with $k_{SRH}^{input} = 10^7$ s^{-1} and $\mu = 10^{-4}$ cm^2 V^{-1} s^{-1}, the inferred recombination rate constant from the TPV time constant $k_{SRH}(\tau_{TPV}) \approx 10^5$ s^{-1} is two orders of magnitude lower (crossed light blue circle in Figure 2a). It is important to note that for $\mu < 10^{-3}$ cm^2 V^{-1} s^{-1}, both $B(\tau_{TPV})$ and $k_{SRH}(\tau_{TPV})$ decrease for higher recombination rate constants; hence, in many cases, single values of $B(\tau_{TPV})$ and $k_{SRH}(\tau_{TPV})$ map to two separate input recombination parameters that differ by orders of magnitude.

Importantly, the experimentally measured range of TPV time constants reported in the literature for different organic solar cells lies within this region (from 10^{-5} to 10^{-7} s), which corresponds in our case to values of $k_{SRH}(\tau_{TPV})$ of (from 10^5 to 10^7 s^{-1}) and $B(\tau_{TPV})$ of (from 10^{-12} to 10^{-10} cm^3 s^{-1}).[25,51,52] Because TPV time constants in this range do not correspond to a unique input recombination rate constant, some prior reports of recombination rate constants based only on TPV measurements may be incorrect. A further discussion on the complexity of properly characterizing the recombination mechanisms in a commonly used OPV device (P3HT:PCBM) is presented in the Supporting Information, section 5. These initial results show that, even in a simplified system, vastly different recombination rate constants can result in the same TPV time constant.

2.2.2. The Evolution of Charge Carrier Profiles during a TPV Decay

To further understand how two different recombination rate constants can result in the same TPV decay rate, we simulated two devices with second-order recombination in which only the

recombination rate constant was varied: a "fast" recombination case with $B^{input} = 10^{-9} cm^3 s^{-1}$ and a "slow" recombination case with $B^{input} = 10^{-11} cm^3 s^{-1}$. For both values of B^{input} the simulated TPV decay was very similar with $B(\tau_{TPV}) \approx 10^{-11} cm^3 s^{-1}$ (Figure S1, Supporting Information, and light blue star symbols in Figure 2). We extracted the evolution of the excess charge carrier density generated by the laser pulse from the simulations and plotted this average over the whole device versus time as well as corresponding snapshots of the carrier density profiles during the transient.

Figure 3a shows that in the slow recombination case ($B^{input} = 10^{-11} cm^3 s^{-1}$), the average excess carrier density and photovoltage decay have fairly similar dynamics. Moreover, the excess electron and hole profiles across the intrinsic layer are relatively uniform (Figure 3b), confirming that the photovoltage decay is a good proxy for the dynamics of recombination throughout the active layer.

Figure 3c,d shows the results for the fast recombination case where $B(\tau_{TPV}) \ll B^{input}$. It is noteworthy that the evolution of average excess charge carrier density is considerably different to the excess photovoltage (Figure 3c). The excess charge carrier concentration (Figure 3c, green curve with square markers) initially shows a rapid increase as carriers are generated by the laser pulse (for $t < 0$). As soon as the laser is turned off, the excess charge carrier density in the device decreases significantly in the first 2 μs. This first decay can be fitted with an exponential decay with a time constant of 0.19 μs, that we will refer to as $\tau_{Q,1}$. After this initial fast decay, the charge carrier density decreases with an exponential decay with a time constant of 3.5 μs, that we will refer to as $\tau_{Q,2}$. The excess photovoltage evolution

(Figure 3c, orange curve with triangle markers), on the other hand, increases significantly when the pulse light is turned on and interestingly, continues to increase for more than 300 ns after the pulse as carriers are transferred to the contacts. The photovoltage subsequently decreases with an exponential decay with a time constant of around 3.7 μs. We note that in the fast recombination case, while the time constant of the slow decay of charge carrier density is similar to the photovoltage time constant (Figure S3, Supporting Information), more than 60% of the charge carriers recombined with a time constant that is an order of magnitude lower. Moreover using the fast time constant of the charge carriers $\tau_{Q,1}$ we can estimate a recombination rate constant of $B(\tau_{Q,1}) = 5.3 \times 10^{-10} cm^3 s^{-1}$, which is considerably closer to the input recombination rate constant compared with that extracted from the simulated TPV dynamics, $B(\tau_{TPV}) = 2.2 \times 10^{-11} cm^3 s^{-1}$. $B(\tau_{Q,1})$ in this case is still lower than B^{input}, and the difference between the extracted and input rate constants is due to the use of the average charge carrier density (n_{avg}) in the device as the charge carrier distribution in this case is highly inhomogeneous. Analysis of the evolution of charge carrier profiles at different positions of the device (Figure 3d) reveals that the fast recombination case shows a significantly inhomogeneous evolution as compared with the low recombination case (Figure 3b). During the pulse the excess charge carrier density increases homogeneously across the absorber layer; once the laser pulse is turned off, the charge carrier density in the middle of the absorber decreases significantly. Meanwhile, carriers continue to accumulate in the space-charge region close to the transport layer interfaces for some hundreds of nanoseconds. A similar slow rise time was observed in the simulations presented by
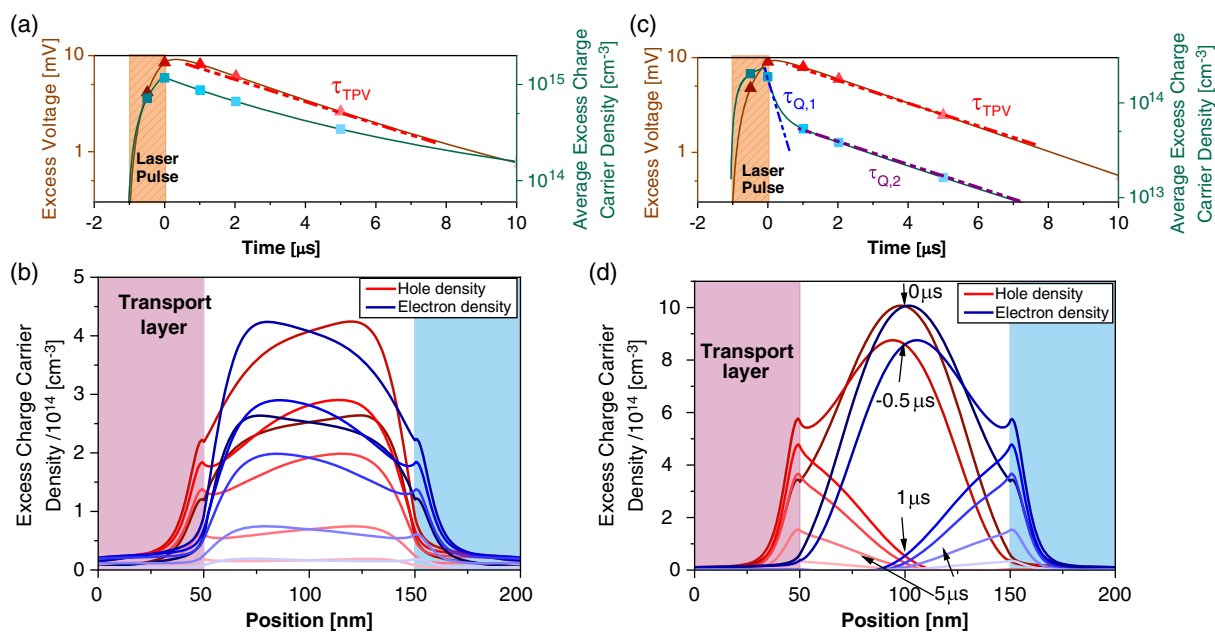

Figure 3. a,c) Photovoltage decay (orange curve, red, and pink markers) and averaged excess charge decay in the device (green curve, blue markers) for a) the slow recombination case and c) the fast recombination case. b,d) Evolution of electron and hole density in the intrinsic layer during the TPV experiment for the b) slow recombination case and d) the fast recombination case. Note that the colors of the lines in panels b and d are identical to the color of the symbols in a and c. The TPV time constant is represented in this plot as τ_{TPV}, the fast charge decay time constant is $\tau_{Q,1}$, and the slow charge decay time constant is $\tau_{Q,2}$ The average charge carrier density at open-circuit voltage for the fast recombination case is $5 \times 10^{15} cm^{-3}$ and for the slow recombination case is $8 \times 10^{15} cm^{-3}$.

Wood et al. and was related to the low conductivity in the active layer.[49] Following this, the carrier density then decays at a rate slower than the initial bulk decay. This inhomogeneous evolution of the charge carriers across the intrinsic layer explains the two different decays of the average charge carrier density. Furthermore, these results show that, for the fast recombination case, the measured photovoltage is only related to redistribution and recombination of charge carrier at the transport layer interfaces as changes in the electrostatic potential are determined by changes in these space-charge regions in accordance with Gauss's Law. The evolution of carriers in these regions is not solely dependent on the recombination rate constant and can be significantly limited by transport, particularly in low-mobility devices.

To summarize the abovementioned results, for the fast and slow recombination cases investigated the evolution of charge carriers during the simulated TPV experiment is significantly different. In the slow recombination case, the charge carrier densities increase and decrease relatively homogeneously across the absorber, resulting in a good agreement between the average charge carrier and photovoltage decays. By contrast, the charge carrier density evolution across the absorber in the fast recombination case exhibits a significant inhomogeneity. Here, charge carriers in the middle of the absorber decay with a time constant $\tau_{Q,1}$, which is an order of magnitude lower than the time constant $\tau_{Q,2}$ of those close to the interfaces. In the latter case the photovoltage decay reflects the evolution of the charges close to the interfaces.

2.2.3. TPV Time Constant and Charge Carrier Lifetime

In the previous section, we showed that where $B^{input} \gg B(\tau_{TPV})$, the average charge carrier density in the device decayed in a biexponential form with a fast time constant ($\tau_{Q,1}$) that was an order of magnitude lower than the slow time constant ($\tau_{Q,2}$). In this particular example we found that $\tau_{Q,1}$ could be used to calculate a recombination rate constant ($B(\tau_{Q,1})$) closer to the true input B^{input}. To evaluate the generality of this observation, we fit the decay of the average excess charge carrier density for all the cases simulated in Figure 1 to a sum of two exponentials to extract $\tau_{Q,1}$ and $\tau_{Q,2}$. For all the cases where the recombination rate estimated from TPV diverged from its expected value, $\tau_{Q,1}$ and $\tau_{Q,2}$ were significantly different. Using $\tau_{Q,1}$ we estimate the recombination rate constants $k_{SRH}(\tau_{Q,1})$ (**Figure 4**a) and $B(\tau_{Q,1})$ (Figure 4b) and show that the input value is strongly correlated with the output value regardless of the input recombination scheme or the mobility of the charge carrier in the absorber.

These results generalize the observation that $\tau_{Q,1}$ is solely dependent on the recombination input properties, differing from τ_{TPV} (Figure 1). The divergence between B^{input} and $B(\tau_{Q,1})$ for the high recombination rate constant results from the highly inhomogeneous charge carrier distributions in the active layer and the use of an average value to calculate $B(\tau_{Q,1})$. By studying the evolution of the charge carrier density for several cases, the same inhomogeneous evolution of the charge carrier density was observed, a fast decay of the carriers in the middle of the absorber and a slower decay for the carriers close to the transport
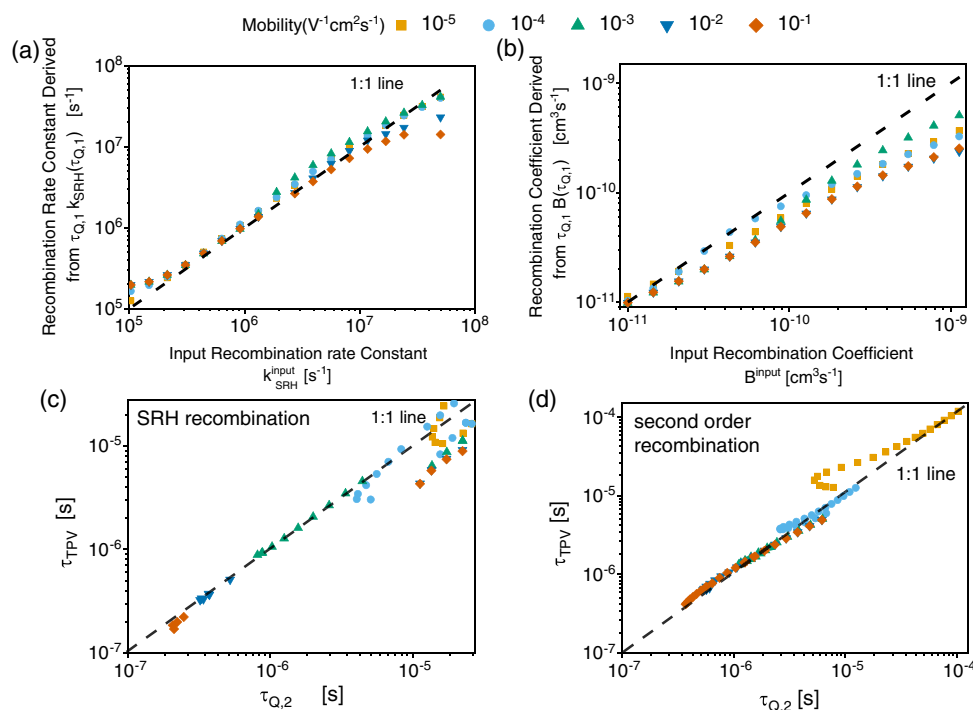

Figure 4. a) Recombination rate $k_{SRH}(\tau_{Q,1})$ extracted from fitting the first decay of charge carrier density against input recombination rate for SRH recombination scheme. b) Recombination rate extracted from fitting the first decay of charge carrier density ($B(\tau_{Q,1})$) against input recombination rate for second-order recombination scheme. c,d) Slow decay component of excess carrier density ($\tau_{Q,2}$) against TPV time constant (τ_{TPV}) for c) SRH recombination and d) second-order recombination case.

Table 1. Change in the fast charge decay time constant ($\tau_{Q,1}$) and TPV time constant (τ_{TPV}) with different change of parameters.

	SRH recombination			Bimolecular recombination		
	τ_{TPV} [µs]	$\tau_{Q,1}$ [µs]	Ratio $\left(\frac{\tau_{TPV}}{\tau_{Q,1}}\right)$	τ_{TPV} [µs]	$\tau_{Q,1}$ [µs]	Ratio $\left(\frac{\tau_{TPV}}{\tau_{Q,1}}\right)$
Reference cell	6.8	0.14	47	3.5	0.15	24
Nonsymmetric mobilities ($\mu_e = 10^{-2}\,\mu_p$)	15	0.15	96	13	0.1	129
High effective density of states ($10^{20}\,cm^{-3}$)	6.6	0.13	50	3.5	0.14	26
Thick device (400 nm)	3.6	0.15	24	3.3	0.13	25
High relative permittivity ($\epsilon = 10$)	12	0.14	86	6.2	0.13	48
Low light intensity ($G = 2.5 \times 10^{20}\,cm^{-3}\,s^{-1}$)	40	0.14	282	11	0.19	57
Nonaligned ETL ($Ec_{ETL} = Ec_l - 0.3\,eV$)	9.1	0.14	66	5.6	0.17	33

layer/absorber interfaces, as shown in Figure 3c. In contrast, Figure 4c,d shows that $\tau_{Q,2}$ is strongly correlated with the time constant extracted from the TPV decay (τ_{TPV}). This confirms that TPV primarily reflects the displacement of the charge carriers in the active layer following an initial fast decay of the charge carriers.

2.2.4. Device Properties and TPV Time Constant

The results presented earlier mainly focus on the effect of the charge carrier mobility in the absorber layer on the correlation between the voltage transient and the recombination rate constant. We now introduce the metric $\tau_{TPV}/\tau_{Q,1}$ to explore the effect of other device parameters on the reliability of the TPV time constant to accurately predict the recombination rate coefficient. Here, values of $\tau_{TPV}/\tau_{Q,1}$ closer to 1 indicate greater reliability of τ_{TPV}.

Taking the case of a fast recombination for both SRH and bimolecular mechanism, with the parameters in Table S1 and S2, Supporting Information, we explored the effect of other parameters on the two lifetimes τ_{TPV} and $\tau_{Q,1}$ and their ratio (**Table 1**). The first thing to note is that for most of the cases considered $\tau_{Q,1}$ hardly changes relative to the reference case, which confirms that $\tau_{Q,1}$ is mainly determined by the change in the recombination rate constant. Considering the second-order recombination case, the change in charge carrier density due to, for example, varying the background light intensity, affects $\tau_{Q,1}$ but not the recombination rate constant $B(\tau_{Q,1})$. On the other hand, τ_{TPV} is strongly affected by several other parameters, such as the carrier mobility in the active layer, the background light intensity, the dielectric constant, etc., and consequently its reliability as a proxy for the recombination rate constant is questionable. For nonsymmetric mobilities, e.g., where the mobility of holes is lower than that of electrons, the increase in TPV time constant suggests that recombination is limited by the transport of the lowest mobility carrier to recombination centers (Table 1). In contrast, the effective density of states at the conduction and valence band edges do not affect $\frac{\tau_{TPV}}{\tau_{Q,1}}$ significantly. Increasing the thickness of the absorber layer has a beneficial effect on the correlation, especially for the first-order (SRH) recombination scheme, where the TPV time constant is half that of the thin-layer case. Increasing the dielectric constant or decreasing the light intensity both appear to have a detrimental effect on the correlation (see Table 1).

3. Analytical Solution

Gathering all the results of the simulations earlier, we have shown that τ_{TPV} depends on different device parameters in addition to the charge carrier recombination rate constant and charge carrier density. The charge carrier decay in the fast recombination case in Figure 3c, shows that the average charge carrier decay during the TPV experiment is not described by a simple monoexponential decay, but rather a biexponential decay that reflects the inhomogeneous charge recombination inside the device (Figure 3d). The charge carriers in the bulk of the absorber decayed with a time constant ($\tau_{Q,1}$), an order of magnitude faster than the charge carriers close to the transport layer ($\tau_{Q,2}$). The first time constant was shown to be a good measure of the input recombination rate constant for the majority of the cases simulated in Figure 4, whereas the second time constant was similar to τ_{TPV}. These observations emphasize that τ_{TPV} is related to the charge carriers close to the interfaces between the transport layers and the absorber. To understand what controls the TPV time constant for the cases where it is not close to its expected input value, our analysis now focuses on this interfacial region.

Figure S2, Supporting Information, shows that at open circuit, the electric field at the interface is not negligible and is larger in the fast recombination case as compared with the slow recombination case. Moreover, the inhomogeneous evolution of charge carriers in the absorber layer simulated in the fast recombination case (Figure 3d) suggests that to properly understand the charge carrier decay the displacement of the charge must be included in the analysis. The effect of the charge carrier displacement on the TPV time constant has previously been accounted for by considering its impact on the capacitance of the device.[31,32] In this work, we aim to relate the TPV time constant to input parameters of the drift-diffusion model. To this end, we solved the time-dependent drift-diffusion equations at the absorber–ETL interface. The same arguments can be equally applied to the absorber–HTL interface. We will focus our analysis on the case where the charge carrier near the interface would have to move back to the centre of the device to recombine. Discrepancies between the TPV time constant and $\tau_{Q,1}$ are caused by such charge carrier redistributions in the devices. Thus, in what follows we refer to these cases as transport-limited cases. Our analysis additionally assumes the following approximations: 1) The density of electrons is much higher than that of holes at the absorber–ETL interface; 2) The considered region is large

enough such that the electric field falls to zero far from the inter-face (i.e. in the middle of the absorbed layer); 3) The electric field does not change significantly at the interface during excitation (small perturbation); and 4) Recombination is dominated by second-order processes. Notwithstanding point 4, the same analysis could be applied for a first-order process. Under these assumptions, the change in the excess charge carrier density Δn as a function of position x and time t can be expressed in terms of the generation rate G and the TPV time constant τ_{TPV} as

$$\Delta n(x,t) = \frac{dT(x)}{dx}\exp\left(-\frac{t}{\tau_{tpv}}\right) \quad (1)$$

where the function $T(x)$ is given by

$$T(x) = C\exp\left(-\left(\frac{\sqrt{\frac{G}{B^{input}}}}{\epsilon\epsilon_0 k_B T}\right)^{0.5} x\right)\sin\left(\frac{\pi}{4}\frac{x}{x_{max}}\right) \quad (2)$$

The derivation for Equation (1) and (2) is presented in the Supporting Information, section 6. The TPV time constant is found to be

$$\tau_{TPV} = \frac{q\epsilon\epsilon_0}{\sqrt{\frac{G}{B^{input}}}\mu} \quad (3)$$

which depends on both the charge carrier density at open circuit ($n_{OC} = \sqrt{G/B^{input}}$) and the charge carrier mobility μ. Equation (3) can also be written in terms of the conductivity of the absorber layer at open circuit at different light intensities ($\sigma \propto \sqrt{G/B^{input}}\mu \propto n_{OC}\mu$). Using the same analysis for an SRH recombination scheme, in the limiting case (where the recombination can be approximated as a first-order process) we find

$$\tau_{TPV} = \frac{q\epsilon\epsilon_0 k_{SRH}^{input}}{G\mu} \quad (4)$$

In both solutions for τ_{TPV}, the dependence on true charge dynamics of the TPV time constant is the inverse of that expected for the charge carrier recombination lifetime. As discussed previously, the TPV rate constant can be related to the recombination rate constant via $\tau_{TPV} = (2k_{SRH}(\tau_{TPV}))^{-1}$ for a first-order recombination case and $\tau_{TPV} = (2B(\tau_{TPV})n_{avg})^{-1}$ for a second-order recombination case. The results of the analytic solution presented earlier agree with the results shown in Figure 2 for the high recombination rate cases. **Figure 5** shows the different regimes for the TPV experiment in the case where the first-order recombination dominated and the mobility of the charge carrier is fixed to 10^{-4} cm^2 V^{-1} s^{-1}. The slope of the TPV time constant with the input recombination rate constant slightly diverges from the results of Equation (4), but they overall show the same trend.

In **Figure 6**, the TPV time constant obtained from 500 different simulations (where the input parameters were varied within the ranges shown in Table S7, Supporting Information) is compared with the analytical approximation given by Equation (3) using the input parameters. The results include variations in the charge carrier mobility in the absorber layer, the generation rate, and second-order recombination rate coefficient. All points shown in Figure 6 are taken from the cases where the time constant from
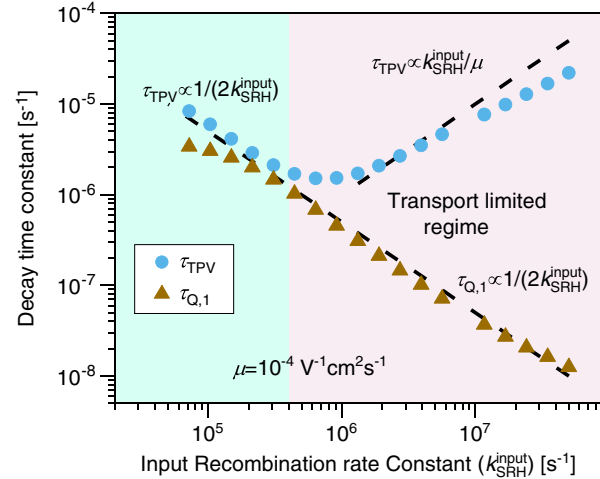

Figure 5. Different regimes of the TPV time constant compared with the lifetime of charge carrier recombination in the bulk for the first-order case presented in Figure 2 and 3 with a mobility of charge carrier in the absorber of 10^{-4} cm^2 V^{-1} s^{-1}.

TPV is more than a factor of 5 higher than the fast recombination time constant of charge carriers. While for high generation rates the analytic and simulation values are strongly correlated, there is a noticeable deviation with low generation rates. This is because many of the assumptions made do not hold for these cases, especially the field-free assumption far from the interface as the thickness of the active layer considered is 100 nm (which is a common thickness of the active layer of OPV devices).

To cross check the results, values for B^{input} were obtained from the simulations using the recombination rate constant extracted using the fast decay of the charge carriers $B(\tau_{Q,1})$, and the TPV time constant was used to recalculate the mobility of the slowest charge carrier using Equation (3). The results are compared with the actual mobility input into the simulation in Figure 6b. Overall, the input and back-calculated values are well correlated (correlation coefficient $r \approx 0.9$). However, the relatively large scatter of the estimated mobility indicates that this technique has limited precision, particularly with low carrier generation rates.

From Figure 6, we conclude that the TPV time constant for the transport-limited cases is well approximated by the expression in Equation (3), confirming that, under the given assumptions, TPV time constant is a measure of how fast the charge carriers move back from the transport layer–absorber interface to the centre of the absorber to recombine. This result also provides evidence that the assumptions underlying the analytic solution are well justified, considering that the use of realistic parameters for the drift-diffusion simulation gives similar time constants to those predicted by the analytic solution. Furthermore the results in Figure 6 support the theory that the evolution of charge carriers near the interface during TPV, for the cases where the recombination rate constant extracted from TPV is different from the input recombination rate constant, is attributable to charge carriers that accumulated near the interface during the laser pulse, which then have to move back to the centre of the absorber to recombine. This explains why τ_{TPV} is inversely proportional to the conductivity of the absorber ($\sigma = \sqrt{G/B^{input}}\mu$). In addition,
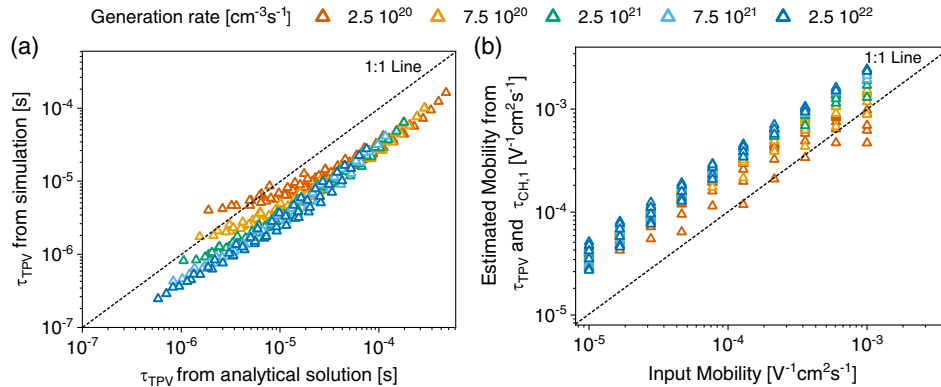
Figure 6. a) TPV time constant from the analytic model compared with the numerical one. b) The estimated mobility from the analytical model compared with the mobility input in the simulation. The two graphs are for second-order recombination processes.

we find that τ_{TPV} is affected by the energy-level alignment at the interface between the transport layer and the absorber (Table 1), suggesting that the thermal activation of the charge carriers over a barrier would affect τ_{TPV}.[53]

Using the derived Equation (3) and (4) we can explain the trend observed in Figure 1a,b. Both equations show a dependence of the TPV time constant on the generation rate constant in the active layer (G). For the SRH recombination case (Equation (4) and Figure 1a), the low light intensities in Figure 1a are all in the transport-limited regime. The simulated TPV time constant follows the trend inferred from Equation (4), i.e. the TPV time constant decreases with increasing generation rate and increasing charge carrier mobility. For higher light intensities, when the TPV time constant calculated using Equation (4) is lower than the true recombination time constant ($2/k_{SRH}^{input}$), the simulated TPV time constant converges to the true value. For the second-order recombination case, the relative difference in the TPV time constant between the three devices at a similar generation rate appears to be independent of the generation rate considered. In Equation (3), the TPV time constant is proportional to the inverse square root of the generation rate constant ($\sqrt{G^{-1}}$), and the expected recombination time constant is $(2B(\tau_{TPV})n_{avg})^{-1}$. If we consider that $n_{avg} \approx \sqrt{G/B^{input}}$ (uniform generation rate and uniform charge carrier distribution in the active layer), then both the time constant in Equation (3) and the recombination time constant are dependent on the inverse square root of the generation rate constant ($\sqrt{G^{-1}}$).

The results of this first part show that τ_{TPV} can be used to estimate the true recombination lifetime only in very limited cases. However, we have also shown that if $\tau_{Q,1}$ can be accurately measured in addition to τ_{TPV}, the recombination properties of the absorber can be accurately characterized. To do so, we have developed an adapted experimental CE technique that allows the reliable measurement of the bulk recombination lifetime.

4. TPQ: A Novel Technique to Probe Charge Carrier Recombination in Devices

Following the previous analysis, it is clear that a technique capable of directly monitoring the cell's charge carrier density following a

perturbation would be a more reliable measure of the device's recombination kinetics than measuring the TPV. Techniques such as TDCF[6] and TRCE[9] measure the charge carrier density in the devices at different times by integrating the current extracted when switching to short circuit or negative biases. In TDCF, a cell is left under a voltage bias in the dark; then, at the start of the measurement ($t = 0$ s), a short laser pulse is used to excite the sample. The photogenerated charge carriers are measured at different delay times by summing the collected carriers before and after switching the cell to a negative bias. The evolution of the total collected carriers gives information concerning the recombination kinetics of the device.[6,7] The inferred recombination properties of the device from TDCF measurements have been shown to be affected by the low charge carrier mobility of the device.[54] TRCE on the other hand is performed under light bias and at open circuit. At $t = 0$ s, the light bias is turned off and charge is extracted after a time delay by switching the cell to short circuit.[9,14] Both these techniques are large perturbation methods as compared with TPV which is a small perturbation technique. Using a similar method to these techniques we developed TPQ, a novel time-delayed CE technique to probe the charge carrier concentration during TPV decay and measure a reliable charge carrier recombination lifetime.

Figure 7 shows the TPQ experimental timeline with the following sequence: 1) The cell is kept under optical bias at open circuit and the photovoltage is monitored. 2) At time $t = 0$ s, a laser pulse of length t_{laser} is used to excite the device. 3) After a delay time t_{delay} the cell is switched to short circuit and the bias light is simultaneously switched off (<200 ns switching time). 4) The transient current response is recorded and integrated to obtain the extracted charge density. As with a CE experiment, the integrated current corresponds to the difference between the illuminated and dark carrier densities inside the device.

By subtracting the charge carrier density extracted from the cell without the laser pulse (i.e., a conventional CE experiment) from the measured charge carrier density at different t_{delay}, the change in the excess charge carrier density injected by the laser pulse can be quantified. The proposed experiment was simulated for the slow and fast recombination cases. The results (Figure S7, Supporting Information) demonstrate that this experiment indeed correlates well with the charge carrier decay and can
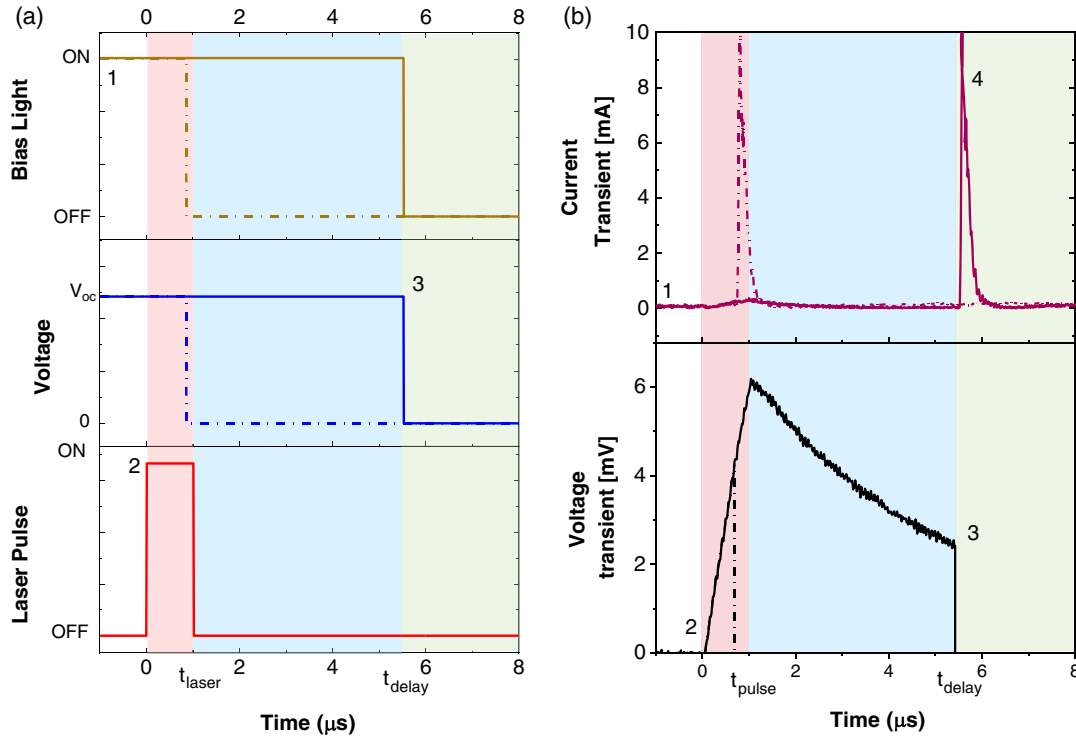
ADVANCED
SCIENCE NEWS
www.advancedsciencenews.com

Solar
RRL
www.solar-rrl.com

Figure 7. a) TPQ experimental timeline and (b) measured quantities during the experiment. 1-the cell is kept under optical bias at open circuit. 2—the cell is excited with a laser pulse of length t_{pulse}. 3—the light bias is switched off and the cell is switched to short circuit after a delay t_{delay}. 4—The current transient is measured. The dashed lines show the case where the CE occurs during the laser pulse.

distinguish whether the TPV signal probes the bulk recombination time constant ($\tau_{Q,1}$) or the slower, transport-limited recombination ($\tau_{Q,2}$). When a 0.3 μs switching delay is included in the simulation, however, the initial carrier decay cannot be resolved: only the second decay is monitored by the measurement (Figure S7, Supporting Information). This result indicates that a switching time of <0.1 μs of the cell's open-/closed-circuit condition and bias light is critical to achieving an accurate measurement of the recombination kinetics with this technique. This limitation is primarily due to the parallel plate capacitance of the cell and is therefore dependent on the dimensions of the active layer. To circumvent possible errors in the experiment and extend the use of TPQ to devices with faster recombination kinetics, we investigated the charge carrier concentration evolution during the laser pulse. In this measurement the laser pulse is kept on for the same duration (t_{laser}) regardless of whether the cell is at short circuit or open circuit. Consequently, in cases where CE occurs before the end of the laser pulse, excess carriers are generated during CE. Consequently, the measurement accounts for both the charge generated while the device is at open and short circuit. The extracted charge

$$n_{ce}(t) = \begin{cases} n_{ce,sc}(t_{laser} - t) + n_{ce,OC}(t); & 0 < t < t_{laser} \\ n_{ce,OC}(t); & t_{laser} < t \end{cases} \quad (5)$$

is the sum of these two charge densities, $n_{ce,SC}$ and $n_{CE,OC}$, extracted at short circuit and open circuit, respectively. By assuming the recombination of charge to be insignificant at short

circuit, $n_{ce,SC}$ can be compared with $n_{CE,OC}$ to quantify the charges lost due to recombination during the laser pulse. By simulating the TPQ experiment during and after the pulse for the fast and slow recombination cases (Figure S8, Supporting Information) it is clear that for the fast recombination cases, most of the charge carriers excited by the laser (almost 90%) recombine during the pulse. Furthermore, the charge carrier decay is faster during the laser pulse than after it. From this observation, we propose that the excess charge carriers during the pulse recombine with the fast time constant ($\tau_{Q,1}$) whereas carriers after the pulse recombine with the time constant $\tau_{Q,2}$. This assumption is valid in the cases where $\tau_{Q,1} \ll \tau_{Q,2}$ and the laser pulse length t_{laser} verifies $\tau_{Q,1} < t_{laser} \ll \tau_{Q,2}$ (derivation in Supporting Information). Following these assumptions and considering the derivation in the Supporting Information we find for the extracted charge

$$n_{ce}(t) = \begin{cases} n_{laser} \times \left(1 - \frac{t}{t_{laser}} + \frac{\tau_{Q,1}}{t_{laser}}\left(1 - \exp\left(-\frac{t}{\tau_{Q,1}}\right)\right)\right); & 0 < t < t_{laser} \\ n_{ce,OC}(t_{laser})\left(\exp\left(-\frac{t}{\tau_{Q,2}}\right)\right); & t_{laser} < t \end{cases}$$
$$(6)$$

Here, n_{laser} is the excess charge carrier density injected by the laser, t_{laser} is the laser pulse length, and $n_{ce,OC}(t_{laser})$ is the excess charge extracted following the pulse. Using Equation (6), the decay of $n_{ce}(t)$ during and after the pulse can be fit to obtain $\tau_{Q,2}$ and $\tau_{Q,1}$.

5. Experimental Results

5.1. Validation of the TPQ Experimental Technique

As a means to verify this new technique experimentally, we measured TPQ on a typical polymer: nonfullerene acceptor (P3HT:O-IDTBR) device.[55] We selected this device because some reports based on TPV analysis suggested that recombination was slow compared with fullerene devices.[55] The TPQ response of the devices under 0.1 suns bias illumination is shown in **Figure 8**. The results in Figure 8a show that after the laser pulse the dynamics of the CE phase (blue circle markers) are comparable with the TPV transient (green triangle markers). Due to the limited switching time resolution of the measurement however, the initial fast decay cannot be resolved properly (inset in Figure 8a). By contrast, the decay of the charge carrier concentration during the laser pulse (blue circle markers) shows that more than 90% of the photoinjected charges recombine during the laser pulse (Figure 8). This result suggests that most of the charge carriers excited by the laser pulse decay faster than the observed decay of the photovoltage. By fitting Equation (5) to the charge carrier decay over the whole period (Figure 8b), a short recombination time constant of 0.3 μs was obtained for $t < t_{pulse}$ as compared with the time constant of 5 μs for $t > t_{pulse}$.

In Equation (5), two parameters are solely dependent on the experimental setup: the laser pulse length and the laser pulse intensity. It follows that the accuracy of the extracted lifetime can be further improved by measuring over a range of pulse lengths and intensities. Supporting Information, section 10 includes a short guide on how to carry out the TPQ measurement and under what conditions the measurement is reliable, considering both the assumptions made for the fit as well as the experimental limitations. To summarize the laser pulse length should be long enough to probe the fast recombination of the charge carriers, and the laser power intensity should be low enough to ensure that the measurement is in the small perturbation regime.

5.2. Comparison of TPV and TPQ Measurements on P3HT-Based Devices

To test the TPQ method and address the question of how replacing PCBM with O-IDTBR affects recombination dynamics in P3HT-based solar cells, TPQ and TPV were measured for two bulk heterojunction devices based on P3HT as the donor and PCBM or O-IDTBR as the acceptor. TPQ and TPV were measured under different background light intensities to extensively compare their results under different conditions. The TPV time constant at 1 sun was measured to be 13 μs for P3HT:O-IDTBR compared with 3.4 μs for P3HT:PCBM (**Figure 9**). Tellingly, the carrier lifetimes measured by TPQ were significantly lower at 0.3 and 1.5 μs, respectively. The difference between the TPQ and the TPV time constant supports the conclusion from the simulations, i.e. that the TPV time constant is limited by charge transport from the interface to the bulk to recombine and that the majority of the charge carriers recombine with a faster lifetime. On the other hand, the recombination of the charge carrier after the pulse ($\tau_{Q,2}$) was similar to the photovoltage decay (τ_{TPV}), confirming the validity of the simulation results for the different light intensities and different blends.

By comparing the two blends, both the TPV and the TPQ time constants were higher for the P3HT:PCBM blend. In this instance, both devices show the same trend for both TPV and TPQ data. However previously the TPV time constant of the P3HT:O-IDTBR blend was reported to be larger than that of the P3HT:PCBM blend[56] in contrast to our observations. The difference between our finding and the previous report is not surprising, considering the observed dependence of the TPV time constant on different parameters (Table 1). Moreover, $\tau_{Q,1}$ for the P3HT:PCBM device tends to a constant value for light intensities below 0.5 suns, indicating that the dominant recombination mechanism is first order at those light intensities. At higher light intensities, second-order recombination appears to dominate (Figure S9, Supporting Information). The P3HT:O-IDTBR blend shows a linear
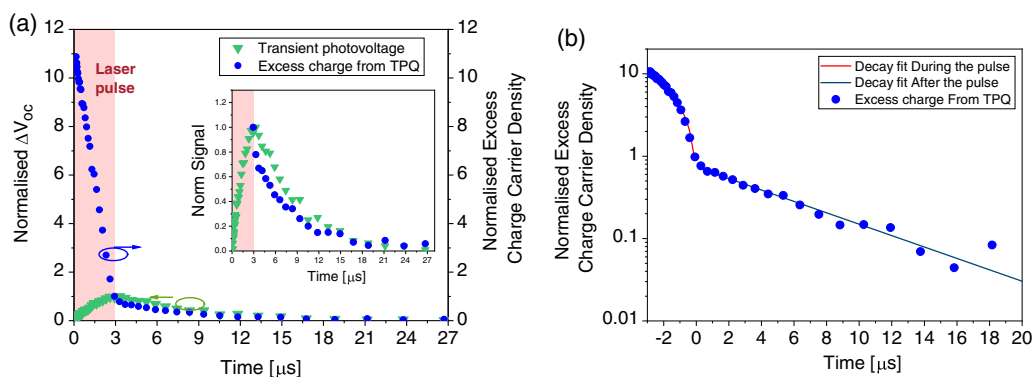

Figure 8. a) Excess charge carrier density obtained from the TPQ experiment and TPV for a P3HT: OIDTBR device under light intensity equivalent to 0.1 sun. Both the excess charge carrier density and the TPV are normalized to their value at the end of the laser pulse. The large difference between the charge density extracted during and after the laser pulse confirms that the majority of the laser-generated charge carriers recombine faster than the photovoltage decay. The inset focuses on the behavior for $t > t_{pulse}$. b) Fit of the charge carrier decay for the P3HT:OIDTBR device under light intensity equivalent to 0.1 sun using Equation (5); this results in $\tau_{Q,1} = 0.3$ and $\tau_{Q,2} = 5$ μs.
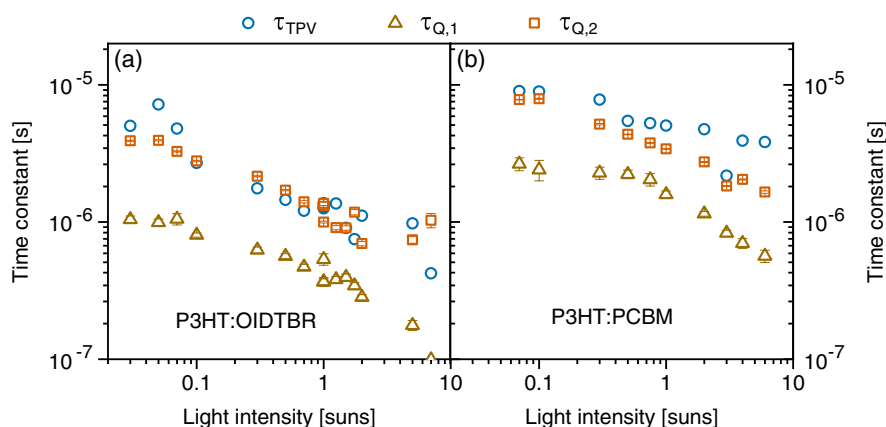
Figure 9. Time constant (TPV time constant (τ_{TPV}), fast TPQ constant ($\tau_{Q,1}$), and slow TPQ time constant ($\tau_{Q,2}$)) for a range of bias light intensities from 0.02 to 8 suns for a) a P3HT:O-IDTBR device and b) a P3HT:PCBM device.

decay of the carrier lifetime with light intensity, indicating that $\tau_{Q,1}$ versus light intensity power law remains approximately constant and the same recombination mechanism dominates.

Using the background carrier density (n_0) measured using CE under constant light bias and assuming that for both devices the dominant recombination mechanism around 1 sun is second order, the second-order recombination coefficient was calculated to be $4.8 \pm 1 \times 10^{-11}\,cm^3\,s^{-1}$ for the PCBM device and $4.6 \pm 0.5 \times 10^{-10}\,cm^3\,s^{-1}$ for the O-IDTBR device using the TPQ measurement of the fast time constant ($\tau_{Q,1}$). Furthermore, using the plot of $\tau_{Q,1}$ against n_0 for different light intensities (Figure S9, Supporting Information), we extract a reaction order around 1 sun light intensity of almost 2 for the P3HT:PCBM device and 1.8 for P3HT:O-IDTBR. We further discuss the use of the two techniques TPV and TPQ to extract the mobility of the active layer in the Supporting Information, Section 11.

5.3. Comparison of TPV and TPQ Measurements of High-Efficiency Nonfullerene Acceptor-Based Devices

Having demonstrated the use of TPQ on the prototypical P3HT-based devices, we now move to apply the technique to more recently developed, high-efficiency nonfullerene-based devices. The three different systems investigated were PTB7-Th:IEICO-4F, PFBDB-T:C8-ITIC, and PDBDT-2F:C8-ITIC (full names of the molecules are given in Supporting Information, section S13) and were fabricated using established recipes.[57–59] The performance of the devices measured under simulated AM1.5G illumination is shown in Table S12, Supporting Information, with the PTB7-Th:IEICO-4F blend showing an efficiency of above 11%, the PFDBD-T:C8-ITIC blend an efficiency of 12%, and the PBDB-T:C8-ITIC an efficiency of 8.2%. These performances are comparable with existing published results.[57]

Figure 10 shows the carrier lifetime measured using both TPV and TPQ over a range of light intensities for the three blends.
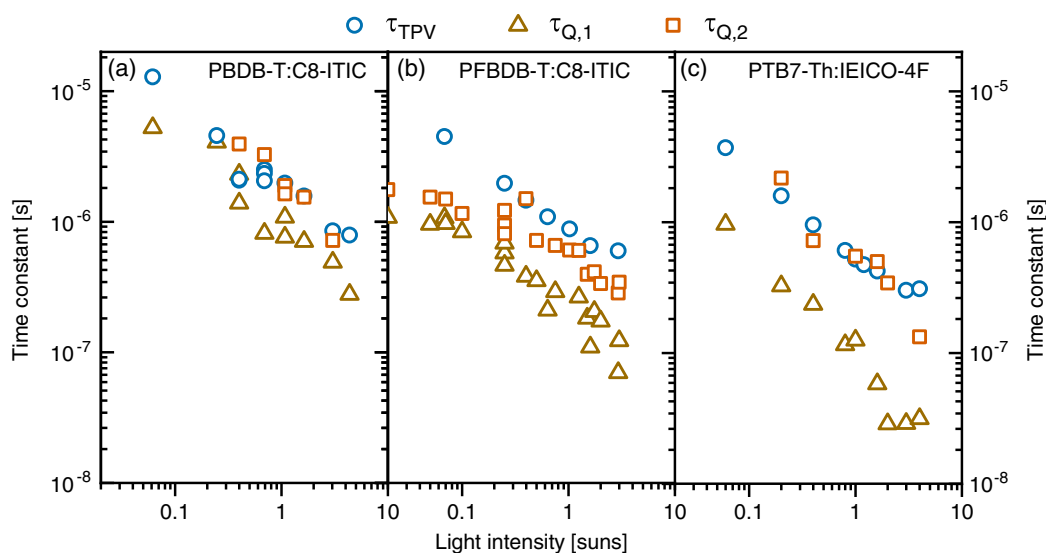

Figure 10. Time constant (TPV time constant (τ_{TPV}), fast TPQ constant ($\tau_{Q,1}$), and slow TPQ time constant ($\tau_{Q,2}$)) for a range of bias light intensities from 0.05 to 8 suns for a) a PDFBDT-2F:C8-ITIC device, b) a PDBD-T:C8-ITIC device, and c) a PTB7-Th:IEICO-4F device.

We note first that $\tau_{Q,1}$ is lower than τ_{TPV} for the three blends considered, with the PBDB-T:C8-ITIC blend showing the lowest difference between the two values. For the other blends (PFDBD-T:C8-ITIC and PTB7-Th:IEICO-4F), the differences between $\tau_{Q,1}$ and τ_{TPV} are considerable, with the TPV time constant at 1 sun 1 ± 0.3 μs for PFDBD-T:C8-ITIC and 0.5 ± 0.1 μs for PTB7-Th:IEICO-4F, whereas the carrier lifetimes measured by TPQ ($\tau_{Q,1}$) were 0.2 ± 0.1 μs and 0.1 ± 0.05 μs, respectively, i.e. almost an order of magnitude lower. These results show that even for high-efficiency blends, the TPV lifetime does not accurately reflect the recombination lifetime of the charge carriers in the bulk of the devices, and it is therefore important to use additional techniques such as TPQ to reliably measure the charge carrier recombination lifetime.

To demonstrate the increase in understanding we can gain from TPQ, as opposed to TPV, we briefly compare the life-times of PBDB-T:C8-ITIC, a high energetic offset blend, and PFBDB-T:C8-ITIC, a low energetic offset blend. The lifetimes at 1 sun, show that the lifetimes extracted from TPV are almost identical, giving us little information about the difference in recombination dynamics between the blends. The charge carrier lifetimes extracted from TPQ, however, show that the nonfluori-nated polymer blend shows a larger $\tau_{Q,1}$ compared with the fluorinated blend, as well as a smaller difference between τ_{TPV} and $\tau_{Q,1}$. A larger $\tau_{Q,1}$ in the nonfluorinated blend indicates a slower apparent recombination, which results in the lower difference between τ_{TPV} and $\tau_{Q,1}$ (c.f. Figure 2). This finding implies that the device with the higher open-circuit voltage and higher efficiency shows faster recombination, a conclusion which would not have been possible to reach when measuring only TPV. This work emphasizes the value of further investigation into the rela-tionship between energetic offsets at bulk heterojunctions and charge recombination rates.

6. Conclusion

In this work, we have explored the validity of using TPV to extract the charge carrier recombination lifetime in solar cells, or more precisely, the validity of the correlation between the evolution of the excess photovoltage and the excess charge carrier concentra-tion inside the absorber. Using drift-diffusion simulations, we established that under many circumstances the change in the voltage measured at the external contacts and the excess charge carrier evolution inside the absorber layer were very dissimilar. In these cases, the excess photovoltage was found to be related to the accumulation and recombination of charge in the space-charge regions at the absorber–transport layer interfaces. The evolution of carriers in this region was found to be controlled by various device properties including the mobility and relative permittivity of the absorber, and the bias light intensity.

By studying the charge carrier decay during the TPV experi-ment for different simulated devices, we observed a significant difference between the input recombination rate coefficient and that extracted using the TPV time constant. The average excess carrier density inside the absorber was found to decay inhomo-geneously, with a fast decay component related to the recombi-nation of carriers in the middle of the absorber and a slower decay component related to carriers in the space-charge layer

close to the absorber/transport layer interface. By fitting the decay of the excess charge carrier density using a biexponential decay, we established that the decay of the charge carriers inside the absorber layer is mainly governed by the fast recom-bination mechanism. Its time constant $\tau_{Q,1}$ could be used to gain reliable information on the recombination rate constant and mechanisms. From this observation, we developed a comple-mentary experiment (TPQ) that probes the excess charge carrier concentration inside devices during the TPV experiment. For four of the five different device systems studied, P3HT:PCBM, P3HT:O-IDTBR, PFDBD-T:C8-ITIC, and PTB7-Th:IEICO-4F, the lifetime of the charge carriers inferred from TPQ was 3–5 times faster than τ_{TPV}, and therefore the recombi-nation rate constant measured from the TPV experiment is significantly smaller than the actual recombination rate constant of the devices. This new technique can therefore be used inde-pendently to more accurately characterize the recombination mechanism of the charge carriers at different light intensity con-ditions for a variety of OPV systems in addition to other types of thin-film solar cells.

This work shows how a simple analysis of the results of TPV can be misleading and that extra care should be taken before drawing any conclusion on the properties of an absorber layer using this technique alone. Further, the information gained from the simulation results led us to develop a new characterization technique will can prove to be useful to measure the recombina-tion properties of different thin-film devices. In particular, we anticipate that TPQ will prove useful for understanding the behavior of recently developed high-efficiency OPV devices.

7. Experimental Section

Drift-Diffusion Model: A 1-D drift-diffusion model was implemented to simulate the results using MATLAB's built-in partial differential equation solver for parabolic and elliptic equations (pdepe). The full details can be found in a study by Calado et al.[42] This model was used to simulate TPV, *J–V* characteristics, and the delayed CE measurements. For all the simu-lations we fixed the carrier densities at the boundaries to be the same as that of the transport layers in equilibrium.

TPV was simulated using a symmetric model to allow the cell to be at open-circuit conditions, as described in a study by Calado et al.[42] The laser length and light intensity were varied to keep the cell in the small perturbation regime, where the transient open-circuit voltage did not exceed 30 mV. We used a uniform generation profile throughout the active layer of the device to simulate the bias light.

In all cases TPV measurements were simulated using a 0.2 μs pulse superimposed on the constant background illumination of the same inten-sity. The photovoltage was then monitored during the system's relaxation to its quasithermal equilibrium.

Optoelectronic Characterization (Setup): The TPV and TPQ experiments were conducted in nitrogen atmosphere. Variable, continuous intensity illumination was provided using a ring of 1 W white Lumiled light-emitting diodes (LEDs) incident on the indium thin oxide (ITO) side of the device. For the TPV experiment, once the device output reached a steady state, the device was perturbed using a single diffuse pulse from a PhoxX 638-150 laser diode, the intensity of which was adjusted for each background light bias intensity to ensure that the system was in the small perturbation regime. The resulting voltage transient $\Delta V(t)$ ($\Delta V \ll V_{OC}$) was measured at the contacts using a DPO 5104B Tektronix digital phosphor oscillo-scope. The 1 MΩ input impedance of the oscilloscope was used to hold the device at approximately open circuit throughout the measurement. Output transients were fitted to a single exponential function to obtain

the time constant of the voltage decay. For the TPQ experiment, the cell was switched from open-circuit to short-circuit using a metal–oxide–semiconductor field-effect transistor (MOSFET) (ZVN4306A) controlled using an AFG3102C Tektronic pulse generator. The same signal from the pulse generator was used to control a MOSFET (ZVN4306A) that switched off the LED ring. The current from the device was measured using the DPO 5104B Tektronix digital phosphor oscilloscope with a 46 Ω resistance. The excess current was measured by subtracting the signal without the laser pulse, and the delay time between the laser pulse and the switch to short circuit was ensured using the two outputs of the pulse generator.

J–V Characterization: Current–voltage characteristics were measured using a Keithley 236 source-measure unit under AM1.5 solar irradiation (Oiel 300W solar simulator) at an intensity of 100 mW cm^{-2}. All electrical measurements were carried out in nitrogen atmosphere.

Devices Fabrication: P3HT:O-IDTBR blends were prepared on prepatterned ITO-covered glass substrates. After cleaning, ZnO was deposited from a zinc acetate anhydrous solution (110 mg mL^{-1} in 2-methoxyethanol with 30 μL ethanolamine per 1 mL) by spin coating at 4000 rpm, followed by annealing at 200 °C. The blend was dissolved in chlorobenzene at a ratio of 1:1 and a concentration of 24 mg mL^{-1} and was then spin cast at a spin speed of 2000 rpm in nitrogen atmosphere and subsequently soft-annealed at 130 °C for 10 min after spin coating. The thicknesses of the active layers were 80–100 nm. To complete the devices, MoO$_3$ (10 nm) and silver (100 nm) were evaporated through shadow masks to yield devices with an area of 4.5 mm^2. P3HT batches were purchased from Sigma Aldrich.

P3HT:PCBM blends were prepared on prepatterned ITO-covered glass substrates. After cleaning, PEDOT:PSS was deposited by spin coating at 3000 rpm, followed by annealing at 140 °C for 15 min. The blend was dissolved in chlorobenzene at a ratio of 1:1 and a concentration of 18 mg mL^{-1}. The blend was spin cast at spin speeds of 700 rpm in nitrogen atmosphere and was soft annealed at 110 °C for 10 min after spin coating. To complete the devices, Ca (10 nm) and Al (80 nm) were evaporated through shadow masks to yield devices with an area of 4.5mm^2. PCBM batches were purchased from Sigma Aldrich.

PFBDB-T, PBDB-T and C8-ITIC were synthesized following established procedures in reference.[57] PFBDB-T:C8-ITIC and PBDB-T:C8-ITIC devices were synthesized according the recipe in reference.[57] In brief, PFBDB-T:C8-ITIC and PBDB-T:C8-ITIC solutions were prepared by dissolving the materials at 20 mg mL^{-1} in chlorobenzene at a ratio of 1:1.25, donor to acceptor, followed by stirring on a hotplate at 50 °C in nitrogen atmosphere.

PTB7-th and IEICO-4F were purchased from 1-material and PTB7-th:IEICO-4F blends were made according to a previous study,[58] by dissolving the materials at a ratio of 1:1.15 at 20 mg mL^{-1} in chlorobenzene, with 4% added chloronaphtalene.

PFBDB-T:C8-ITIC, PBDB-T:C8-ITIC, and PTB7-Th:IEICO-4F thin films were fabricated by spin casting their respective solutions at 2000 rpm (PFBDB-T:C8-ITIC and PBDB-T:C8-ITIC) or 1000 rpm (PTB7-Th:IEICO-4F) onto ZnO thin films fabricated in the same manner as earlier, and the devices were completed with the evaporation of MoO$_3$ and Ag cathode, as mentioned earlier.

Supporting Information

Supporting Information is available from the Wiley Online Library or from the author.

Acknowledgements

Conflict of Interest

The authors declare no conflict of interest.

Keywords

[1] J. Nelson, *The Physics of Solar Cells*, Imperial College Press, London **2003**.
[2] U. Rau, U. W. Paetzold, T. Kirchartz, *Phys. Rev. B Condens. Matter Mater. Phys.* **2014**, *90*, 035211.
[3] W. Shockley, H. J. Queisser, *J. Appl. Phys.* **1960**, *1640*, 510.
[4] W. K. Metzger, I. L. Repins, M. Romero, P. Dippo, M. Contreras, R. Noufi, D. Levi, *Thin Solid Films* **2009**, *517*, 2360.
[5] C. G. Shuttle, B. O'Regan, A. M. Ballantyne, J. Nelson, D. D. C. Bradley, J. de Mello, J. R. Durrant, *Appl. Phys. Lett.* **2008**, *92*, 093311.
[6] J. Kniepert, I. Lange, N. J. Van Der Kaap, L. J. A. Koster, D. Neher, *Adv. Energy Mater.* **2014**, *4*, 301401.
[7] J. Kniepert, M. Schubert, J. C. Blakesley, D. Neher, *J. Phys. Chem. Lett.* **2011**, *2*, 700.
[8] J. Mort, I. Chen, A. Troup, M. Morgan, J. Knights, R. Lujan, *Phys. Rev. Lett.* **1980**, *45*, 1348.
[9] T. M. Clarke, J. Peet, P. Denk, G. Dennler, C. Lungenschmied, A. J. Mozer, *Energy Environ. Sci.* **2012**, *5*, 5241.
[10] T. M. Clarke, C. Lungenschmied, J. Peet, N. Drolet, A. J. Mozer, *Adv. Energy Mater.* **2015**, *5*, 1401345.
[11] B. Wright, Y. Nakajima, T. M. Clarke, K. Okuda, H. Paananen, *Adv. Energy Mater.* **2017**, *7*, 1602026.
[12] A. J. Mozer, N. S. Sariciftci, L. Lutsen, D. Vanderzande, R. Österbacka, M. Westerling, G. Juška, *Appl. Phys. Lett.* **2005**, *86*, 112104.
[13] A. Baumann, T. J. Savenije, D. H. K. Murthy, M. Heeney, V. Dyakonov, C. Deibel, *Adv. Funct. Mater.* **2011**, *21*, 1687.
[14] N. W. Duffy, L. M. Peter, R. M. G. Rajapakse, K. G. U. Wijayantha, *J. Phys. Chem. B* **2000**, *104*, 8916.
[15] J. E. Mahan, D. L. Barnes, *Solid. State. Electron.* **1981**, *24*, 989.
[16] J. Bisquert, A. Zaban, M. Greenshtein, I. Mora-Seró, *J. Am. Chem. Soc.* **2004**, *126*, 13550.
[17] W. L. Leong, S. R. Cowan, A. J. Heeger, *Adv. Energy Mater.* **2011**, *1*, 517.
[18] D. Klotz, D. S. Ellis, H. Dotan, A. Rothschild, *Phys. Chem. Chem. Phys.* **2016**, *18*, 23438.
[19] B. C. O'Regan, F. Lenzmann, *J. Phys. Chem. B* **2004**, *108*, 4342.
[20] J. P. Correa-Baena, W. Tress, K. Domanski, E. H. Anaraki, S. H. Turren-Cruz, B. Roose, P. P. Boix, M. Grätzel, M. Saliba, A. Abate, A. Hagfeldt, *Energy Environ. Sci.* **2017**, *10*, 1207.
[21] B. C. O'Regan, P. R. F. Barnes, X. Li, C. Law, E. Palomares, J. M. Marin-Beloqui, *J. Am. Chem. Soc.* **2015**, *137*, 5087.
[22] G. S. Han, H. S. Chung, B. J. Kim, D. H. Kim, J. W. Lee, B. S. Swain, K. Mahmood, J. S. Yoo, N.-G. Park, J. H. Lee, H. S. Jung, *J. Mater. Chem. A* **2015**, *3*, 9160.

[23] A. Maurano, R. Hamilton, C. G. Shuttle, A. M. Ballantyne, J. Nelson, B. O'Regan, W. Zhang, I. McCulloch, H. Azimi, M. Morana, C. J. Brabec, J. R. Durrant, *Adv. Mater.* **2010**, *22*, 4987.

[24] D. Baran, T. Kirchartz, S. Wheeler, S. Dimitrov, M. Abdelsamie, J. Gorman, R. S. Ashraf, S. Holliday, A. Wadsworth, N. Gasparini, P. Kaienburg, H. Yan, A. Amassian, C. J. Brabec, J. R. Durrant, I. McCulloch, *Energy Environ. Sci.* **2016**, *9*, 3783.

[25] Y. Cao, A. Stavrinadis, T. Lasanta, D. So, G. Konstantatos, *Nat. Energy* **2016**, *1*, 16035.

[26] A. Classen, T. Heumueller, I. Wabra, J. Gerner, L. He, L. Einsiedler, N. Li, G. J. Matt, A. Osvet, X. Du, A. Hirsch, C. J. Brabec, *Adv. Energy Mater.* **2019**, *9*, 1902124.

[27] N. Y. Doumon, M. V. Dryzhov, F. V. Houard, V. M. Le Corre, A. Rahimi Chatri, P. Christodoulis, L. J. A. Koster, *ACS Appl. Mater. Interfaces* **2019**, *11*, 8310.

[28] T. Kirchartz, J. Nelson, *Phys. Rev. B Condens. Matter Mater. Phys.* **2012**, *86*, 165201.

[29] L. Xie, S. Yoon, Y. J. Cho, K. Kim, *Org. Electron.* **2015**, *25*, 212.

[30] N. Gasparini, X. Jiao, T. Heumueller, D. Baran, G. J. Matt, S. Fladischer, E. Spiecker, H. Ade, C. J. Brabec, T. Ameri, *Nat. Energy* **2016**, *1*, 16118.

[31] D. Kiermasch, A. Baumann, M. Fischer, V. Dyakonov, K. Tvingstedt, *Energy Environ. Sci.* **2018**, *11*, 629.

[32] O. J. Sandberg, K. Tvingstedt, P. Meredith, A. Armin, *J. Phys. Chem. C* **2019**, *123*, 14261.

[33] M. Neukom, S. Züfle, S. Jenatsch, B. Ruhstaller, *Sci. Technol. Adv. Mater.* **2018**, *19*, 291.

[34] O. Breitenstein, *IEEE J. Photovoltaics* **2014**, *4*, 899.

[35] C. G. Shuttle, R. Hamilton, J. Nelson, B. C. O'Regan, J. R. Durrant, *Adv. Funct. Mater.* **2010**, *20*, 698.

[36] T. C. M. Müller, B. E. Pieters, U. Rau, T. Kirchartz, *J. Appl. Phys.* **2013**, *113*, 134503.

[37] I. Zonno, A. Martinez-Otero, J.-C. Hebig, T. Kirchartz, *Phys. Rev. Appl.* **2017**, *7*, 034018.

[38] U. Wurfel, A. Cuevas, P. Wurfel, *IEEE J. Photovoltaics* **2015**, *5*, 461.

[39] S. Schäfer, A. Petersen, T. A. Wagner, R. Kniprath, D. Lingenfelser, A. Zen, T. Kirchartz, B. Zimmermann, U. Würfel, X. Feng, T. Mayer, *Phys. Rev. B* **2011**, *83*, 165311.

[40] T. Kirchartz, B. E. Pieters, J. Kirkpatrick, U. Rau, J. Nelson, *Phys. Rev. B* **2011**, *83*, 115209.

[41] R. C. I. MacKenzie, C. G. Shuttle, M. L. Chabinyc, J. Nelson, *Adv. Energy Mater.* **2012**, *2*, 662.

[42] P. Calado, A. M. Telford, D. Bryant, X. Li, J. Nelson, B. C. O'Regan, P. R. F. Barnes, *Nat. Commun.* **2016**, *7*, 13831.

[43] C. Eames, J. M. Frost, P. R. F. Barnes, B. C. O'Regan, A. Walsh, M. S. Islam, *Nat. Commun.* **2015**, *6*, 7497.

[44] P. Bhattacharya, *Semiconductor Optoelectronic Devices*, Prentice Hall, Upper Saddle River, NJ **1994**.

[45] W. Shockley, W. T. Read, *Phys. Rev.* **1952**, *87*, 835.

[46] S. Hubbard, *Photovoltaic Solar Energy* (Eds: A. Reinders, P. Verlinden, W. van Sark, A. Freundlich), John Wiley & Sons, Ltd, Chichester, UK **2017**, pp. 39–46.

[47] B. C. Regan, S. Scully, A. C. Mayer, E. Palomares, J. Durrant, *J. Phys. Chem.* **2005**, *109*, 4616.

[48] D. Rauh, C. Deibel, V. Dyakonov, *Adv. Funct. Mater.* **2012**, *22*, 3371.

[49] S. Wood, J. C. Blakesley, F. A. Castro, *Phys. Rev. Appl.* **2018**, *10*, 24038.

[50] S. Kobayashi, T. Takenobu, S. Mori, A. Fujiwara, Y. Iwasa, *Appl. Phys. Lett.* **2003**, *82*, 4581.

[51] D. Credgington, J. R. Durrant, *J. Phys. Chem. Lett.* **2012**, *3*, 1465.

[52] Y. Shao, Y. Yuan, J. Huang, *Nat. Energy* **2016**, *1*, 1.

[53] R. T. Tung, *Phys. Rev. B* **1992**, *45*, 13509.

[54] U. Würfel, M. Unmüssig, *Sol. RRL* **2018**, *2*, 1800229.

[55] S. Holliday, R. S. Ashraf, A. Wadsworth, D. Baran, S. A. Yousaf, C. B. Nielsen, C. H. Tan, S. D. Dimitrov, Z. Shang, N. Gasparini, M. Alamoudi, F. Laquai, C. J. Brabec, A. Salleo, J. R. Durrant, I. McCulloch, *Nat. Commun.* **2016**, *7*, 1.

[56] N. Gasparini, M. Salvador, T. Heumueller, M. Richter, A. Classen, S. Shrestha, G. J. Matt, S. Holliday, S. Strohm, H.-J. Egelhaaf, A. Wadsworth, D. Baran, I. McCulloch, C. J. Brabec, *Adv. Energy Mater.* **2017**, *7*, 1701561.

[57] Z. Fei, F. D. Eisner, X. Jiao, M. Azzouzi, J. A. Röhr, Y. Han, M. Shahid, A. S. R. Chesman, C. D. Easton, C. R. McNeill, T. D. Anthopoulos, J. Nelson, M. Heeney, *Adv. Mater.* **2018**, *30*, 1705209.

[58] X. Song, N. Gasparini, L. Ye, H. Yao, H. Hou, H. Ade, D. Baran, *ACS Energy Lett.* **2018**, *3*, 669.

[59] H. Yao, Y. Cui, R. Yu, B. Gao, H. Zhang, J. Hou, *Angew. Chemie Int. Ed.* **2017**, *56*, 3045.